Signal-Intensity Informed Multi-Coil MRI Encoding Operator for Improved Physics-Guided Deep Learning Reconstruction of Dynamic Contrast-Enhanced MRI

Demirel, Omer Burak; Yaman, Burhaneddin; Moeller, Steen; Weingartner, Sebastian; Akcakaya, Mehmet

DOI
10.1109/EMBC48229.2022.9871668

Publication date
2022

Document Version
Final published version

Published in
2022 44th Annual International Conference of the IEEE Engineering in Medicine & Biology Society (EMBC)

2022 44th Annual International Conference of
the IEEE Engineering in Medicine & Biology Society (EMBC)
Scottish Event Campus, Glasgow, UK, July 11-15, 2022

2022 44th Annual International Conference of the IEEE Engineering in Medicine & Biology Society (EMBC) | 978-1-7281-2782-8/22/$31.00 ©2022 IEEE | DOI: 10.1109/EMBC48229.2022.9871668

Signal-Intensity Informed Multi-Coil MRI Encoding Operator for Improved Physics-Guided Deep Learning Reconstruction of Dynamic Contrast-Enhanced MRI

Ömer Burak Demirel[1,2], Burhaneddin Yaman[1,2], Steen Moeller[2],
Sebastian Weingärtner[1,2,3] and Mehmet Akçakaya[1,2]

***Abstract*— Dynamic contrast enhanced (DCE) MRI acquires a series of images following the administration of a contrast agent, and plays an important clinical role in diagnosing various diseases. DCE MRI typically necessitates rapid imaging to provide sufficient spatio-temporal resolution and coverage. Conventional MRI acceleration techniques exhibit limited image quality at such high acceleration rates. Recently, deep learning (DL) methods have gained interest for improving highly-accelerated MRI. However, DCE MRI series show substantial variations in SNR and contrast across images. This hinders the quality and generalizability of DL methods, when applied across time frames. In this study, we propose signal intensity informed multi-coil MRI encoding operator for improved DL reconstruction of DCE MRI. The output of the corresponding inverse problem for this forward operator leads to more uniform contrast across time frames, since the proposed operator captures signal intensity variations across time frames while not altering the coil sensitivities. Our results in perfusion cardiac MRI show that high-quality images are reconstructed at very high acceleration rates, with substantial improvement over existing methods.**

I. INTRODUCTION

Dynamic contrast-enhanced (DCE) MRI is widely used in different organs, including the heart, kidney, prostate, breast, brain, among others [1], [2]. These acquisitions typically require snap-shot imaging of the whole anatomy during or after the administration of an exogenous contrast agent. High spatio-temporal resolution and sufficient coverage are crucial in DCE MRI to capture the contrast uptakes adequately [3], [4]. However, data acquisition times still remain a major challenge, requiring trade-offs between coverage and spatio-temporal resolution, and necessitating accelerated MRI.

In DCE MRI applications, parallel imaging, simultaneous multi-slice (SMS) imaging and compressed sensing (CS) are the most commonly used acceleration methods [5]–[7]. Recently, physics-guided deep learning (PG-DL) has gained substantial interest in accelerated MRI to improve reconstruction quality [8]–[11]. At higher acceleration rates, where conventional methods exhibit aliasing and noise artifacts, PG-DL is able to provide high-quality reconstructions [9]–[12]. However, several challenges hinder the utility of PG-DL methods for DCE MRI. Typically, PG-DL methods are applied to individual time frames, but they face challenges with generalizability across varying SNRs [13], which is inherently the case across time frames in DCE MRI. While reconstructing individual time frames is preferable to avoid temporal blurring, spatio-temporal regularization has been popular in CS methods in DCE MRI [6], [7]. An analogous training for spatio-temporal PG-DL reconstruction may also be challenging due to differences in contrast uptakes/breathing patterns among different individuals, especially in patient populations, along with the difficulty of obtaining sufficiently large training databases for DCE MRI acquisitions.

In this work, we propose the use of a signal-intensity informed multi-coil (SIIM) encoding operator for improving PG-DL reconstruction of highly-accelerated DCE MRI acquisitions. SIIM encoding operator captures the SNR/signal-intensity variations across time frames, leading to a more uniform contrast across the image series, which in turn facilitates generalizability for DL methods. The proposed approach was applied to highly-accelerated perfusion cardiac MRI. Comparisons were made to split slice-GRAPPA, locally low-rank (LLR) regularized reconstruction [14]–[16], and PG-DL with a conventional multi-coil encoding operator, where the proposed method visibly outperformed all in terms of image quality.

II. METHODS

A. Physics-Guided Deep Learning MRI Reconstruction

The inverse problem for MRI reconstruction is given as:

$$\hat{\mathbf{x}}_{reg} = \arg\min_{\mathbf{x}} ||\mathbf{y}_\Omega - \mathbf{E}_\Omega \mathbf{x}||_2^2 + \mathcal{R}(\mathbf{x}), \tag{1}$$

where $\mathbf{y_\Omega}$ is the acquired multi-channel k-space, Ω is the in-plane undersampling pattern, $\mathbf{x}$ is the image of interest, $\mathbf{E_\Omega}$ is the multi-coil encoding operator and $\mathcal{R}(\cdot)$ is the regularizer. Note the first quadratic terms enforces data consistency (DC) with the acquired points. Using variable splitting with quadratic penalty [11], [17], the objective function in (1) can be decoupled in two sub-problems:

$$\mathbf{z}^{(t)} = \arg\min_{\mathbf{z}} \mu \|\mathbf{x}^{(t-1)} - \mathbf{z}\|_2^2 + \mathcal{R}(\mathbf{z}), \tag{2}$$

$$\mathbf{x}^{(t)} = \arg\min_{\mathbf{x}} \|\mathbf{y}_\Omega - \mathbf{E}_\Omega \mathbf{x}\|_2^2 + \mu \|\mathbf{x} - \mathbf{z}^{(t)}\|_2^2, \tag{3}$$

where μ is the penalty parameter, and $\mathbf{z}^{(t)}$ and $\mathbf{x}^{(t)}$ are intermediate and reconstructed images at t^{th} iteration, respectively. PG-DL unrolls (2) and (3) for a fixed number of

[1]Department of Electrical and Computer Engineering, [2]Center for Magnetic Resonance Research, University of Minnesota, Minneapolis, MN, USA, and [3]Department of Imaging Physics, Delft University of Technology, Delft, Netherlands. e-mails: {demir035, yaman013, moell018, sweingae, akcakaya}@umn.edu

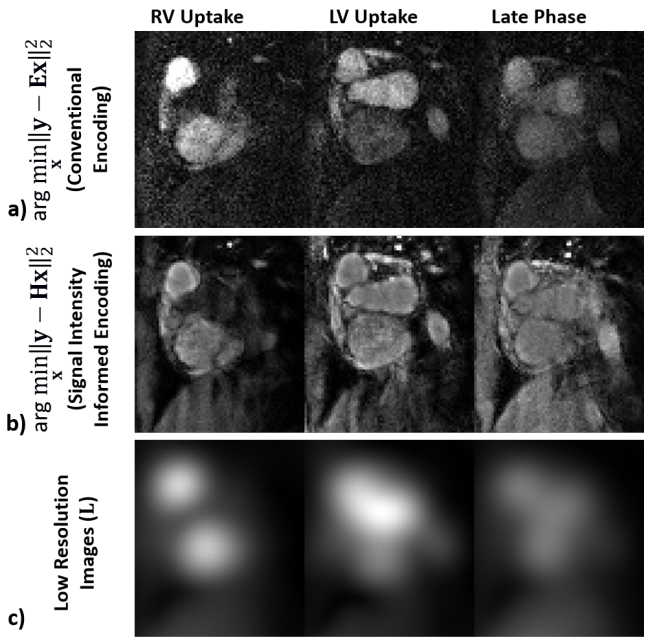

Fig. 1: Unregularized least squares estimate of a representative slice using: a) conventional operator using ESPIRiT and b) proposed SIIM encoding operator. Visible SNR/signal intensity changes are seen in (a), while uniform contrast using (b). c) Low-resolution images ($\mathbf{L}$) for the slice of interest for three different time frames. The product of middle and bottom rows yield contrast similar to top row, as detailed in (7).

iterations [8]. DC problem in (3) is solved by linear methods, while (2) is solved implicitly using a neural network.

B. Conventional Multi-Coil MRI Encoding Operator

The forward encoding operator $\mathbf{E}$ in (1) is given as [18]:

$$\mathbf{E}_\Omega = \begin{bmatrix} \mathbf{F}_\Omega \mathbf{C}_1 \\ \vdots \\ \mathbf{F}_\Omega \mathbf{C}_K \end{bmatrix}, \tag{4}$$

where $\mathbf{F_\Omega}$ is a partial Fourier operator sampling the pattern Ω, and $\mathbf{C}_k$ is a diagonal matrix representing the sensitivity profile of the k^{th} coil. In many applications, including PG-DL, sensitivity maps are estimated using ESPIRiT [19]. ESPIRiT maps are normalized, i.e. $\sum_k |\mathbf{C}_k|^2 = \mathbf{I}$. Thus for the inverse problem in (1), the SNR variations in the measurements, $\mathbf{y}_\Omega$ across time frames are dynamically exhibited in the solution $\hat{\mathbf{x}}_{reg}$, leading to image outputs with substantially different SNR/signal-intensities across time frames.

C. Proposed Signal Intensity Informed Multi-coil (SIIM) Encoding Operator

Let $\mathbf{L}$ be a diagonal matrix whose entries correspond to the pixel values of an image that corresponds the signal variation in a particular time frame. We define the SIIM operator as:

$$\mathbf{H}_\Omega = \mathbf{E_\Omega L}, \tag{5}$$

and the corresponding inverse problem is now:

$$\hat{\mathbf{x}}_{SIIM} = \arg\min_{\mathbf{x}} ||\mathbf{y}_\Omega - \mathbf{H}_\Omega \mathbf{x}||_2^2 + \mathcal{R}(\mathbf{x}). \tag{6}$$

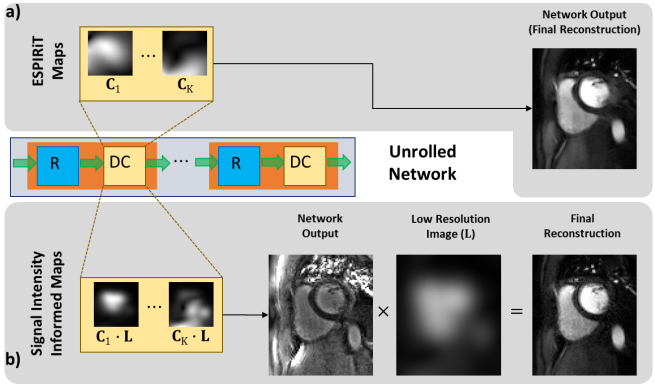

Fig. 2: Physics-guided DL with (a) Conventional operator with ESPIRiT and (b) Proposed SIIM encoding operator. The network outputs are different between conventional and SIIM encoding operators. The product of $\mathbf{L}$ yields the similar contrast as in conventional output.

In the absence of a regularizer, it is easy to show that [20]:

$$\begin{aligned} \hat{\mathbf{x}}_{reg} &= (\mathbf{E}_\Omega^* \mathbf{E}_\Omega)^{-1} \mathbf{E}_\Omega^* \mathbf{y}_\Omega \\ &= \left((\mathbf{L}^{-1})^* \mathbf{H}_\Omega^* \mathbf{H}_\Omega \mathbf{L}^{-1}\right)^{-1} (\mathbf{L}^{-1})^* \mathbf{H}_\Omega^* \mathbf{y}_\Omega \\ &= \mathbf{L}\left(\mathbf{H}_\Omega^* \mathbf{H}_\Omega\right)^{-1} \mathbf{H}_\Omega^* \mathbf{y}_\Omega = \mathbf{L} \cdot \hat{\mathbf{x}}_{SIIM}. \end{aligned} \tag{7}$$

Thus, while the SIIM operator leads to an output, $\hat{\mathbf{x}}_{SIIM}$ with a uniform signal intensity (Fig. 1) compared to the output corresponding to the conventional operator, $\hat{\mathbf{x}}_{reg}$, the two are equivalent once the former is multiplied by $\mathbf{L}$ for the unregularized case.

A simple way to capture the signal intensity variations for a given time frame is to let the diagonal entries of $\mathbf{L}$ correspond to a low-resolution image from the central k-space. In the original parallel imaging setting, a similar concept was utilized by using low-resolution images from the central k-space as coil maps, instead of normalizing them with their root-sum-squares [20]. In this work, the alternative formulation in Eq. (5) enables a more synergistic combination with ESPIRiT map estimation.

There are two main differences between the conventional and SIIM encoding operators. There are numerical differences between solving the objective functions in (1) and (6), which may overcome numerical instabilities resulting from high accelerations, even in the unregularized case [20]. The SIIM formulation also has a further advantage in the regularized setting since the solution to the objective function in (6), $\hat{\mathbf{x}}_{SIIM}$ has a more uniform/flat signal intensity across time frames (Fig. 1). In turn, this may allow improved generalizability for PG-DL reconstructions , since their performance have been shown to be affected by SNR variations of the underlying solutions. Schematics of unrolled networks employing conventional and SIIM encoding operators are depicted in Fig. 2. Notably for the latter type of network, the output has to be multiplied by $\mathbf{L}$ to yield the desired final reconstruction.

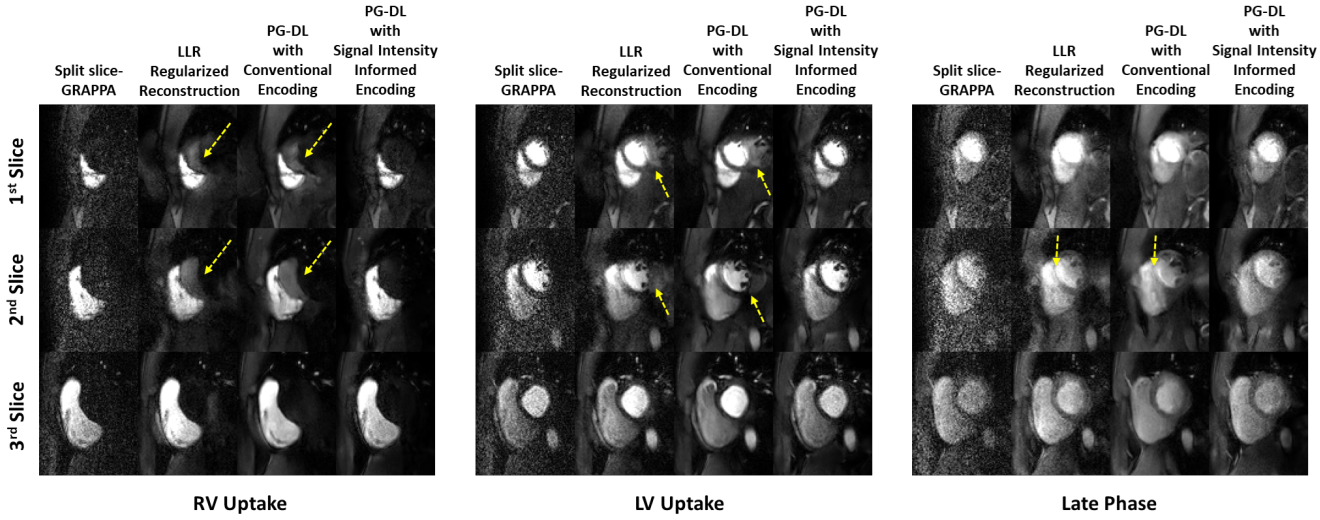

Fig. 3: Representative perfusion CMR results across different time frames on a test subject, acquired with a simultaneous multi-slice factor of 3 and in-plane acceleration of 4 with 6/8 partial Fourier (16-fold acceleration). Substantial noise amplification is observed in split slice-GRAPPA albeit without aliasing artifacts, LLR regularized reconstruction and PG-DL with ESPIRiT reduce noise amplification but suffer from aliasing artifacts (yellow arrows). Proposed PG-DL reconstruction with SIIM encoding operator shows improved image quality by eliminating noise amplification and aliasing artifacts.

D. Imaging Experiments

Imaging experiments were performed at 3T (Siemens Magnetom Prisma) in 8 subjects. The study was approved by our institutional review board and written informed consents were acquired before each scan. Free-breathing first-pass perfusion cardiac MRI (CMR) was performed with the injection of 0.05 mmol/kg gadobutrol (Gadovist) at 4mL/s followed by a 10-mL saline flush. A saturation-prepared GRE sequence was used along with slab-selective saturation pulses for outer volume suppression (OVS) [21]. Relevant imaging parameters were: SMS acceleration = 3, in-plane acceleration = 4, partial Fourier = 6/8, FOV = $360\times360\text{mm}^2$, resolution = $1.7\times1.7\text{mm}^2$, slice-thickness = 8mm, temporal resolution = 110ms. For SMS imaging, an additional calibration scan was performed: Non-prepared GRE with FOV = $360\times360\text{mm}^2$, resolution = $1.7\times5.6\text{mm}^2$.

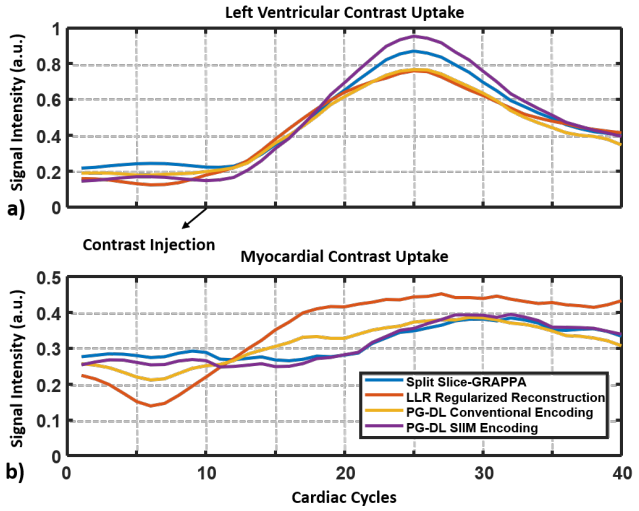

Fig. 4: Representative signal intensity curves showing (a) left ventricular and (b) myocardial contrast uptake. In both cases, split slice-GRAPPA and PG-DL with SIIM encoding operator exhibit similar uptakes. On the other hand, LLR regularized reconstruction and PG-DL with conventional encoding show earlier and different uptakes, which may be a result of the residual aliasing artifacts remaining in these reconstructions.

III. Experiments and Results

A. Implementation Details

SIIM Encoding Operator. Conventional coil sensitivity maps were generated using ESPIRiT [19] and using the 24×24 central part of the calibration scans. For the estimation of low-resolution images, $\mathbf{L}$, the central 24×24 region of each time frame was reconstructed using split slice-GRAPPA [22]. Note that this intermediate reconstruction was necessary due to the SMS encoding, and would not be necessary in single-slice or single-volume imaging. Subsequently, a ringing filter was applied, and smoothing was performed in image domain on each coil image, prior to the generation of the root-sum-of-squares image per time frame. Finally, ESPIRiT maps were multiplied with these low-resolution images as described in Section II-C to generate the SIIM encoding operator.

Self-supervised DL for SMS Reconstruction. For SMS imaging reconstruction, the objective function in (1) is extended to resolve multiple simultaneously excited slices by concatenating the individual slices along the readout direction [23] with an SMS encoding operator that contains individual slice encodings [24], [25]. Since the perfusion acquisitions are highly-undersampled, ground-truth reference data are not available. Therefore, a recently proposed self-supervised learning approach, SSDU [17] was used for training. In particular, in SSDU, the acquired k-space locations, Ω, are split into two disjoint sets, where the first is used in

the DC units of the unrolled network, while the second is used to define training loss [17]. This enabled high-quality network training without requiring ground-truth data.

Network Training Details. Training was done on 4 subjects using 360 SMS k-spaces via unrolling the PG-DL for 10 iterations. A ResNet structure was used for the regularizer and conjugate gradient was used for DC units with the SIIM encoding operator. DC unit itself was unrolled for 20 iterations [11], [17]. Training was performed by using Adam optimizer with a learning rate of $3 \cdot 10^{-4}$. Network was trained to minimize a normalized ℓ_1 - ℓ_2 loss over 100 epochs with a batch size of 1 [17]. Network outputs were multiplied by the respective low-resolution root-sum-squares images (i.e. $\mathbf{L}$) to generate the final reconstruction as described in Section II-C. All training was performed using TensorFlow in Python and processed on a workstation with an Intel E5-2640V3 CPU (2.6 GHz and 256 GB memory), and an NVIDIA Tesla V100 GPU with 32 GB memory. The training takes around 10 minutes per epoch for PG-DL, both with the SIIM encoding operator and the conventional encoding operator.

A separate training with the same parameters and network was performed, except using conventional ESPIRiT maps for the multi-coil encoding operator. This served as the conventional PG-DL reconstruction baseline. Further comparisons were made to split-slice GRAPPA [22], which is a clinically used linear reconstruction strategy for SMS imaging, as well as to LLR regularized reconstruction where the conventional encoding operator was used in the DC term [14]–[16].

B. Reconstruction Results

Fig. 3 shows reconstructed slices for a SMS=3×R=4 accelerated perfusion dataset. Split slice-GRAPPA reconstructed the slices without aliasing artifacts but suffered from high noise amplification. LLR regularized reconstruction and PG-DL with ESPIRiT reduced the noise amplification compared to split slice-GRAPPA, however residual aliasing artifacts deteriorated the image quality in both cases (yellow arrows). Proposed PG-DL with SIIM encoding operator successfully removed the aliasing artifacts while reducing the noise amplification with high image quality during the RV and LV uptakes, as well as later time frames.

Signal intensity curves are depicted in Fig. 4 showing the left ventricular blood pool signal and myocardial contrast uptake from a representative test subject. Split slice-GRAPPA and PG-DL with with SIIM encoding operator follow similar left ventricular contrast uptake, while PG-DL with conventional encoding, and LLR regularized reconstruction show deviations from them. These deviations in quantification for the latter two may be attributed to the residual aliasing artifacts that are visibly apparent in the corresponding reconstructions.

IV. DISCUSSION

We proposed the use of SIIM encoding operator for PG-DL reconstruction of DCE-MRI. The main advantage of this approach is that the output image of the objective function, $\hat{\mathbf{x}}_{SIIM}$ has uniform contrast across different SNRs/time frames, which is critical for addressing the generalization problem in DCE MRI reconstruction. In particular, perfusion CMR has higher SNR in the ventricular uptake time frames, but the SNR slowly depletes especially at later phases.

The SIIM encoding operator leads to a more uniform/flat signal intensity in the output to the corresponding inverse problem in (6) across time frames that have varying SNRs in terms of the acquired k-space. Therefore, regularization operates on more uniform SNRs in the image space, for the corresponding outputs $\hat{\mathbf{x}}_{SIIM}$ regardless of the particular physiological process associated with a time frame. Even though this intermediate solution has more uniform signal intensity, the final reconstruction is generated following multiplication by the corresponding low-resolution image for that time frame. Notably, SIIM encoding operator should not effect the quantification of myocardial perfusion since both conventional and SIIM encoding operations yield the same solution in the absence of a regularizer shown in (7), which is consistent with the quantification of the uptake curves in Fig. 4. On a first look, the approach in (5) may resemble the use of preconditioning in other MRI reconstruction problems [18], [26]. In such settings, preconditioning is typically used to speed up the convergence in solving the data consistency problem in (3). However, the preconditioner does not change the signal intensity variations at the solution output, and the solution to (1) will have similar signal intensity variations across time frames whether preconditioning is used or not. Thus, the SIIM operator is distinct from the typical use of preconditioners in MRI reconstruction, as the former leads to a more uniform/flat signal intensity across different time frames in DCE applications, unlike the latter.

In this study, all the acquisitions were prospectively accelerated, and as such there was no reference image with which to compare the reconstructions. Thus, no quantitative metrics are presented. A reader study is warranted to further evaluate the proposed method, and will be investigated in future studies.

V. CONCLUSIONS

The proposed PG-DL with SIIM encoding operator reconstruction generalizes well across different time frames/SNRs and substantially improves highly-accelerated DCE MRI.

ACKNOWLEDGMENT

This work was partially supported by NIH R01HL153146, NIH P41EB027061, NIH R21EB028369, NSF CAREER CCF-1651825. NWO STU.019.024, 4TU Federation and an AHA Predoctoral Fellowship.

REFERENCES

[1] J. P. O'Connor, P. S. Tofts, et al., "Dynamic contrast-enhanced imaging techniques: CT and MRI," *Br J Radiol*, vol. 84 Spec No 2, pp. S112–120, Dec 2011.

[2] R. M. Mann, C. K. Kuhl, and L. Moy, "Contrast-enhanced MRI for breast cancer screening," *J Magn Reson Imaging*, vol. 50, no. 2, pp. 377–390, 2019.

[3] M. Jerosch-Herold, "Techniques for MR myocardial perfusion imaging," in *J Cardiovasc Magn Reson*, pp. 99–112. Springer, 2019.

[4] P. Sujlana, J. Skrok, and L. M. Fayad, "Review of dynamic contrast-enhanced MRI: Technical aspects and applications in the musculoskeletal system," *J Magn Reson Imaging*, vol. 47, no. 4, pp. 875–890, 2018.

[5] J. K. Yoon, M.-J. Kim, and S. Lee, "Compressed sensing and parallel imaging for double hepatic arterial phase acquisition in gadoxetate-enhanced dynamic liver magnetic resonance imaging," *Invest Radiol*, vol. 54, no. 6, pp. 374–382, 2019.

[6] S. G. Lingala, E. DiBella, and M. Jacob, "Deformation corrected compressed sensing (DC-CS): a novel framework for accelerated dynamic MRI," *IEEE Trans Med Imag*, vol. 34, no. 1, pp. 72–85, 2014.

[7] Y. Yang, C. H. Meyer, F. H. Epstein, C. M. Kramer, and M. Salerno, "Whole-heart spiral simultaneous multi-slice first-pass myocardial perfusion imaging," *Magn Reson Med*, vol. 81, no. 2, pp. 852–862, 2019.

[8] F. Knoll, K. Hammernik, et al., "Deep-learning methods for parallel magnetic resonance imaging reconstruction: A survey of the current approaches, trends, and issues," *IEEE Sig Proc Mag*, vol. 37, no. 1, pp. 128–140, 2020.

[9] K. Hammernik, T. Klatzer, et al., "Learning a variational network for reconstruction of accelerated MRI data," *Magn Reson Med*, vol. 79, pp. 3055–3071, 2018.

[10] J. Schlemper, J. Caballero, J. V. Hajnal, A. N. Price, and D. Rueckert, "A deep cascade of convolutional neural networks for dynamic MR image reconstruction," *IEEE Trans Med Imaging*, vol. 37, no. 2, pp. 491–503, 2017.

[11] H. K. Aggarwal, M. P. Mani, and M. Jacob, "MoDL: Model-based deep learning architecture for inverse problems," *IEEE Trans Med Imaging*, vol. 38, no. 2, pp. 394–405, 2018.

[12] S. A. H. Hosseini, B. Yaman, S. Moeller, M. Hong, and M. Akçakaya, "Dense recurrent neural networks for accelerated MRI: History-cognizant unrolling of optimization algorithms," *IEEE J Sel Top Signal Process*, vol. 14, no. 6, pp. 1280–1291, 2020.

[13] F. Knoll, K. Hammernik, et al., "Assessment of the generalization of learned image reconstruction and the potential for transfer learning," *Magn Reson Med*, vol. 81, no. 1, pp. 116–128, 2019.

[14] J. Yao, Z. Xu, X. Huang, and J. Huang, "An efficient algorithm for dynamic MRI using low-rank and total variation regularizations," *Medical Image Analysis*, vol. 44, pp. 14–27, 2018.

[15] T. Zhang, J. M. Pauly, and I. R. Levesque, "Accelerating parameter mapping with a locally low rank constraint," *Magnetic Resonance in Medicine*, vol. 73, no. 2, pp. 655–661, 2015.

[16] J. Trzasko, A. Manduca, and E. Borisch, "Local versus global low-rank promotion in dynamic mri series reconstruction," in *Proc. Int. Symp. Magn. Reson. Med*, 2011, vol. 19, p. 4371.

[17] B. Yaman, S. A. H. Hosseini, et al., "Self-supervised learning of physics-guided reconstruction neural networks without fully sampled reference data," *Magn Reson Med*, vol. 84, no. 6, pp. 3172–3191, 2020.

[18] K. P. Pruessmann, M. Weiger, P. Börnert, and P. Boesiger, "Advances in sensitivity encoding with arbitrary k-space trajectories," *Magn Reson Med*, vol. 46, no. 4, pp. 638–651, 2001.

[19] M. Uecker, P. Lai, et al., "ESPIRiT—an eigenvalue approach to autocalibrating parallel MRI: where SENSE meets GRAPPA," *Magn Reson Med*, vol. 71, no. 3, pp. 990–1001, 2014.

[20] D. K. Sodickson and C. A. McKenzie, "A generalized approach to parallel magnetic resonance imaging," *Med Phys*, vol. 28, no. 8, pp. 1629–1643, 2001.

[21] S. Weingärtner, S. Moeller, and M. Akçakaya, "Feasibility of ultra-high simultaneous multi-slice and in-plane accelerations for cardiac MRI using outer volume suppression and leakage-blocking reconstruction," in *Proc ISMRM*, 2018.

[22] S. F. Cauley, J. R. Polimeni, H. Bhat, L. L. Wald, and K. Setsompop, "Interslice leakage artifact reduction technique for simultaneous multislice acquisitions," *Magn Reson Med*, vol. 72, no. 1, pp. 93–102, 2014.

[23] O. B. Demirel, S. Weingärtner, S. Moeller, and M. Akçakaya, "Improved simultaneous multislice cardiac MRI using readout concatenated k-space SPIRiT (ROCK-SPIRiT)," *Magn Reson Med*, vol. 85, no. 6, pp. 3036–3048, 2021.

[24] O. B. Demirel, B. Yaman, et al., "20-fold accelerated 7T fMRI using referenceless self-supervised deep learning reconstruction," *arxiv preprint arXiv:2105.05827*, 2021.

[25] O. B. Demirel, B. Yaman, et al., "Improved simultaneous multi-slice functional MRI using self-supervised deep learning," *arxiv preprint arXiv:2105.04532*, 2021.

[26] K. Koolstra, J. van Gemert, P. Börnert, A. Webb, and R. Remis, "Accelerating compressed sensing in parallel imaging reconstructions using an efficient circulant preconditioner for cartesian trajectories," *Magnetic Resonance in Medicine*, vol. 81, no. 1, pp. 670–685, 2019.